Erosion and Confinement of Tungsten in ASDEX Upgrade

R. Dux, A. Janzer, T. Pütterich, and ASDEX Upgrade Team

Max-Planck-Institut für Plasmaphysik, EURATOM Association, D-85748 Garching
e-mail: Ralph.Dux@ipp.mpg.de

Abstract In the fully tungsten clad ASDEX Upgrade, the erosion rates of tungsten have been determined at all relevant plasma facing components using fast spectroscopic measurements. The erosion strongly increases during an edge-localized mode (ELM) and the ELMs are often the dominant cause for erosion. A modeling approach was employed to calculate the erosion at the limiters and the resulting tungsten density at the inside of the H-mode edge transport barrier (ETB). In the ETB, it is assumed that tungsten transport is collisional, i.e. behaves like other impurities [1]. The collisional transport leads to strong inward drifts and steep density gradients in the ETB, which are flattened during an ELM causing an efflux of tungsten. The collisional transport in the ETB is also calculated for typical ITER conditions and the resulting tungsten density profiles are evaluated.

1. Introduction

In a fusion reactor, a central tungsten concentration of only 3×10^{-5} increases the minimum triple product for ignition $nT\tau_E$ by 20% and at 1.9×10^{-4} the ignition condition can not be satisfied [2]. Due to this low concentration limit, a good understanding of the erosion mechanisms, the edge transport, and the radial transport in the confined plasma are mandatory to predict and control the source and the confinement of tungsten. In the fully tungsten clad ASDEX Upgrade, these aspects can be studied. The central impurity transport and the control of central impurity accumulation has previously been investigated [3]. Here, the focus is on the erosion, the penetration into the confined plasma and the transport in the edge transport barrier (ETB) of H-mode plasmas.

In H-mode plasmas with type-I ELMs, the tungsten dynamics at the edge is to a large extent governed by the ELMs. The tungsten production at the plasma facing components is dominated by the erosion during ELMs mainly due to sputtering by light impurities. Nevertheless, discharges with a lower ELM frequency have a higher tungsten concentration in the confined plasma and a minimum ELM frequency is required to perform long steady discharges with constant tungsten concentration. The ELM frequency is usually increased by increasing the deuterium puff level. The flushing of tungsten from the confined plasma during the ELM seems to be the dominant effect compared to the expected increase of tungsten production [4].

The experimental information is gained from spectroscopic measurements. Tungsten influx is measured in the visible spectral range using a WI spectral line at 400.9 nm. Simultaneous measurements on 38 lines-of-sight are used to quantify the influx at all major erosion areas, i.e. the outer divertor, the heat shield at the inner column and the outboard limiters. New measurements of ELM resolved erosion rates, which complement previous local measurements, will be discussed in section 2. The W concentration c_W in the outer part of the confined plasma is deduced from W-spectra in the VUV region. The quasi-continuum at 5 nm emitted by ions around W^{30+} yields c_W at $T_e\approx$1.5 keV, i.e. well within the ETB [5]. Another quasi-continuous spectral feature around 15 nm is presently studied to quantify the concentration of lower ion stages around W^{20+} [6].

It was found that the tungsten source at the outboard limiters has the strongest influence on the tungsten density in the confined plasma. For example, an increase of the limiter source by an outward shift of the plasma column yields an increase of the tungsten density inside the separatrix by a factor of 3, even though the erosion rate at the limiter is offset by a $\approx$20 times stronger divertor rate and a decrease of the $\approx$2 times higher erosion rate at the heat shield [4].

Thus, a modeling approach with an upgraded version of the 1D radial impurity transport code STRAHL was employed to calculate the erosion, penetration and edge transport of tungsten eroded at the limiters.

One important modeling element is the radial impurity transport in the ETB. Here, the density profile evolution of helium, carbon, neon and argon was measured with charge exchange recombination spectroscopy and it was found that between ELMs, all impurities are subject to a strong inward pinch leading to steep impurity density gradients in the ETB which are flattened during an ELM. The evaluated impurity transport coefficients between ELMs are in accordance with neo-classical theory and cause an increase of the peaking with rising impurity charge [7,1]. Thus, we assume also predominantly neo-classical transport for tungsten and find an even stronger peaking than for the light elements. The effect of the ELM is modeled by a strong increase of the diffusion coefficient, which leads to an efflux of impurities from the confined plasma. Since the code models tungsten and light impurities in one run, the efflux of light impurities onto the limiters can be used to self-consistently model the time history of tungsten erosion by physical sputtering and the radial transport of tungsten in the plasma edge. A more detailed version of the paper will follow [8].

2. ELM Resolved Tungsten Erosion Rates

The effect of ELMs on the tungsten influx from the main chamber plasma facing components (PFC) has previously been determined by fast spectroscopic measurements on a single line-of-sight observing one spot in the middle of one low-field side limiter [9] or in the divertor [4]. The total erosion rates can only be estimated, when the poloidal W influx profiles along the PFC are available, which requires measurements on many lines-of-sight for each PFC [4]. However, simultaneous recording of about 10 spectra increases the minimum repetition time of the CCD-cameras to about 4 ms, which is often too slow to have enough data points in the measured time series that are not affected by ELMs. When adding the spectra of all lines-of-sight on the camera into one single bin, the repetition time can be reduced substantially to 0.5 ms for the cameras measuring the limiters and the outer divertor and to 1.2 ms for the camera recording the spectra from the inner column. The calculation of the total influx rate from the binned spectra can be performed when knowing the respective weights of each individual line-of-sight in the binned spectrum, which depend on the influx profiles. Thus, the investigated discharges were performed twice, with slower profile measurements in the first pulse to obtain the required weights.

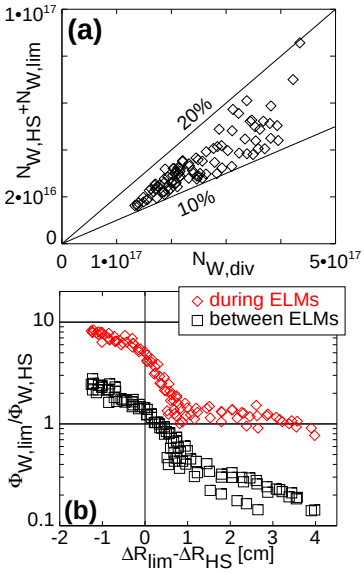

FIG. 1: (a): ELM erosion at the main chamber PFCs versus erosion at the outer divertor. (b): Ratio of the erosion rate at the heat shield to the limiters versus the difference of the distances of the respective component to the separatrix.

A series of type-I ELMy H-mode discharges with I_p=1 MA, B_T=-2.5 T, q_{95}=4.5, P_{NBI}=7.5 MW, P_{ECRH}=1.6 MW and $\langle n_e \rangle$=7.5×10^{19} m^{-3} were performed, which had slow radial shifts of the plasma column, such that either the inner column or the outboard limiters were closer to the separatrix. We designate flux surfaces by ΔR, the radial distance of the flux surface to the separatrix on the low-field side at the height of the magnetic axis and define the distance of a main chamber PFC to the separatrix by the lowest value of ΔR on the poloidal shape of that component. For the limiters, the shifts covered a range ΔR_{lim}=4.2-7.2 cm and for the heat shield ΔR_{HS}=3.2-5.5 cm. The ELM frequency f_{ELM} was varied by applying different deu-

terium puff levels and covers a range f_{ELM}=30-130 Hz. The average energy loss per ELM was in the range ΔW_{ELM}=19-50 kJ.

A database was formed by dividing the tungsten rate evolution during the radial sweeps into intervals of 100 ms length and forming mean values for each interval. An ELM causes a large spike of the influx rate and for each interval, the offset rate Φ_{off} between ELMs was evaluated. The difference to the mean value $\langle\Phi\rangle$ represents the mean rate during ELMs, N_W=$(\langle\Phi\rangle - \Phi_{off})/f_{ELM}$ is the mean number of eroded tungsten atoms per ELM, and c_{ELM}=$(\langle\Phi\rangle - \Phi_{off})/\langle\Phi\rangle$ is the ELM contribution to the total rate, i.e. the fraction of the erosion rate, which is caused by ELMs. Fig.1(a) shows the number of eroded tungsten atoms per ELM for the main chamber components $N_{W,lim} + N_{W,HS}$ versus the eroded atoms in the divertor $N_{W,div}$. In the main chamber, an ELM causes an erosion between (10-20)% of the divertor value. For the ELM influx contribution at the limiters, the ELM erosion dominates and all values are in a range $c_{ELM,lim}$=0.6-0.8 with no trend on ΔW_{ELM} or f_{ELM}, i.e. larger ELMs, which come with lower ELM frequency, contribute as much as faster, lower energy ELMs. There is a trend with ΔR_{lim} and the highest values of $c_{ELM,lim}$ are found at largest ΔR_{lim}. For the heat shield, $c_{ELM,HS}$=0.3-0.5 is found without a clear dependence on ΔW_{ELM} or ΔR_{HS}. These results agree with the earlier local measurement at the limiter, however, at the heat shield we now find for $c_{ELM,HS}$ values which are by 0.2 lower, where the present spectra have much better data quality. In Fig.1(b) rates at the limiters and at the heat shield are compared. It shows the ratio of the respective erosion rates versus the difference of the distances to the separatrix. Positive values of $\Delta R_{lim} - \Delta R_{HS}$ represent plasmas, where the outboard limiters are further away from the separatrix than the heat shield. For the flux between ELMs, $\Phi_{W,lim}/\Phi_{W,HS}$ approximately passes through 1 for about equal distance to the separatrix given the systematic uncertainties of the equilibrium reconstruction (≈(0.5-1) cm) and the flux measurements (factor ≈2-3). However, during ELMs substantially more influx comes from the outboard limiters and the ratio is a factor of 4-5 more weighted towards the limiters. Thus, the ion flux and/or the temperatures, which strongly determine the erosion yield, increase during an ELM much stronger at the outboard components than at the inner column.

3. Impurity Transport Model

Modeling of the impurity transport in principle requires a three dimensional code which includes the impurity production at the limiters and the transport perpendicular and parallel to the magnetic field lines. 3D or 2D codes are computationally very demanding and here, a first approach is done with a 1D impurity transport code. The STRAHL code [10] solves the coupled radial continuity equations for the flux surface averaged densities of each ionised stage of an impurity. The code can model light impurities and tungsten during one run in order get a more realistic description of collisional radial tungsten transport and tungsten erosion during the ELM cycle. For the ASDEX Upgrade runs, carbon and oxygen were included, while for the ITER simulations, helium, oxygen and argon were considered. The background plasma parameters like n_e, T_e and T_i are input parameters to the code, and the main ion density is calculated from the quasi-neutrality condition. For the radial transport, turbulent diffusion coefficients and drift velocities are set ad hoc, while a full treatment of the neo-classical transport parameters is included.

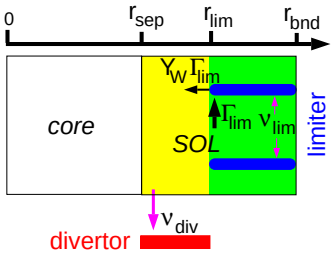

FIG. 2: Sketch of the parallel losses and the tungsten influx in STRAHL.

Outside the separatrix, the parallel transport towards the divertor or to the limiting elements in the main chamber are simply described by volumetric losses. The loss frequency is given by

the parallel connection length between the surface elements and the mean flow velocity of the impurities towards the surfaces. The SOL is divided into a divertor SOL with a large connection length of 50 m and a limiter SOL with 1 m connection length. In the divertor SOL, the collision frequency of the impurities is much larger than the loss frequency, and the impurities are entrained in the deuterium flow, which is described by the adiabatic acoustic ion speed and an average Mach number M. The Mach number M is set ad hoc and constant throughout the entire SOL.

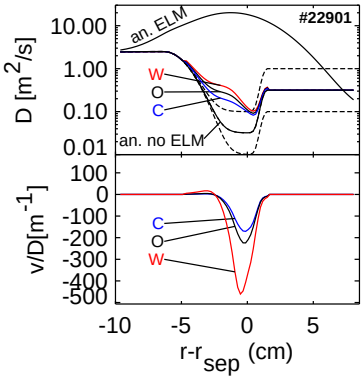

FIG. 3: Profiles of impurity diffusion coefficients and drift parameters for the modeling of AUG discharge #22901.

The neutral impurities start at the limiter tip with r=r_{lim}. They have a constant radial velocity and their density decays radially according to the rate for electron impact ionisation. For the light impurities, the neutral impurity influx rate is set ad hoc to get the desired impurity concentration in the confined plasma. Complete recycling at the limiters can be included by adding the loss rates onto the limiters to the influx. For tungsten, the code calculates the source rate of W using erosion yields for physical sputtering. To this end, the rate of ions that are lost to the limiters is multiplied with the yield $Y_W(E, m)$ and the sum over all charge stages of all elements yields the total influx rate. The yield depends on the energy and the mass of the impinging ions. The energy of the impinging ions is approximated by the value for a collision-less deuterium plasma [11], which yields E=$k_B(2T_i + 3ZT_e)$ for T_i=2T_e. The first term is the average ion energy at the sheath entrance and the second term is due to acceleration within the sheath. The yield is calculated with the revised Bodhansky formula as given in [12]. The energy distribution of the sputtered W atoms is assumed to be a Thompson distribution [13] with a cos-angular distribution. For tungsten, also the fraction of promptly redeposited ions is calculated. These ions immediately return to the surface during the first gyration after ionisation and are removed from the erosion source.

The elements of the radial transport model are depicted in Fig.3. In the phase between ELMs, the anomalous diffusion coefficient was reduced in the ETB to D_{an}^{ETB} being well below the collisional diffusion coefficient of all impurities (solid black line). In Fig.3 it is about a factor of 10 below the collisional values where W has the largest diffusion coefficient. The curves in color show the sum of anomalous and collisional contributions for each element. The drift velocity is purely collisional. The value of the drift parameter v_{neo}/D in this phase are shown in the lower box, where W has the strongest inwardly directed drift parameter. The minimum is just inside the separatrix. From r=r_{sep}+0.5 cm to r=r_{sep}+1.5 cm, the anomalous diffusion coefficient is increased to a second

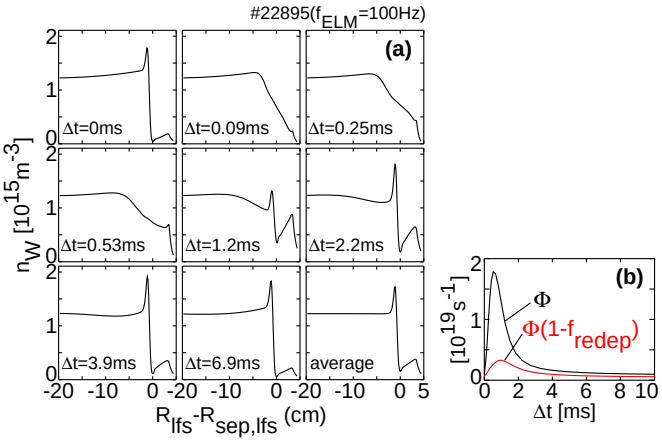

FIG. 4: Fig.(a): The modeled evolution of the total W density n_W during an ELM cycle of 10 ms duration. D_{SOL}=1 m^{2}s^{-1} and D_{an}^{ETB}=0.032 m^{2}s^{-1} was used. The lower right frame shows the temporally averaged profile. Fig.(b) depicts the time evolution of the tungsten sputtering rate Φ and the effective source $\Phi(1 - f_{redep})$.

plateau D_{SOL}. During a sensitivity scan (see below), D_{SOL} and D_{an}^{ETB} was independently varied and the boundaries of the according D_{an} profiles are indicated by the dashed lines. An ELM is induced by a sudden switch-on of a large diffusion coefficient in the edge (upper black curve), which decays linearly in time within 1 ms.

An example of the modeled density evolution of the total tungsten density n_W during an ELM cycle of Δt_{ELM}=10 ms duration for discharge #22895 is shown in Fig.4(a). Here, the settings for the two plateaus of the turbulent diffusion coefficient were D_{SOL}=1 m^{2}s^{-1} and D_{an}^{ETB}=0.032 m^{2}s^{-1}. The radial co-ordinate is the distance to the separatrix at the low-field side equator. All impurities are in quasi-equilibrium, i.e. the temporal average density over an ELM cycle $\langle n \rangle$ is constant in time. The profile of $\langle n_w \rangle$ is depicted in the lower right box and the other boxes show various time points Δt with respect to the start of the ELM. The gradients of the strongly peaked edge profile at Δt=0 ms are flattened in the first few 100 μs after the start of the ELM. At the same time the tungsten sputtering rate Φ rises as is shown in Fig.4(b), however, the prompt redeposition leads to a much smaller increase of the effective source $\Phi(1 - f_{redep})$. After Δt=1 ms, the edge gradient recovers till the start of the next ELM. At a major radius of $\approx$-1.2 cm inside of the separatrix, a peak of the density evolves, which is due to a maximum in the v/D profile with slightly positive (outward directed) value of 17 m^{-1}.

4. Modeling of ASDEX Upgrade H-mode discharges

The model was applied to three discharge phases with different deuterium puff levels Φ_D and ELM frequencies. The model has previously been applied to these discharges [14] in order to find one consistent solution, without studying the dependence on the above mentioned parameters. Another difference with respect to [14] is, that on top of the turbulent D_{SOL}, PS transport coefficients were used within the divertor SOL, which has been avoided in this work.

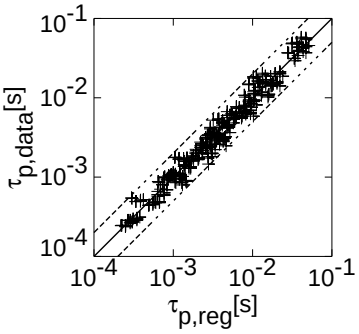

FIG. 5: Regression of the particle confinement time of tungsten τ_p on the ELM frequency, the average parallel loss time from SOL to divertor $\langle\langle \tau_{SOL\to div} \rangle\rangle$ and the SOL diffusion coefficient D_{SOL}. The dashed lines denote a factor of 2 deviation from the regression.

In order to understand the main dependence of the modeled tungsten confinement on the ELM frequency, the perpendicular and parallel transport parameters, an independent scan of the ELM frequency with f_{ELM}=25, 50, 100, and 200 Hz, the inter-ELM anomalous diffusion coefficients D_{an}^{ETB}=0.01, 0.0316 and 0.1 m^{2}s^{-1}, D_{SOL}= 0.1, 0.316 and 1 m^{2}s^{-1}and the average Mach number M=0.033, 0.1 and 0.3 was performed. The transport model for each input parameter set was solved until temporal quasi-equilibrium of all impurities was reached. Finally, the scan was repeated using the background profiles n_e, T_e and T_i of all three discharges. For each setting, the particle confinement time of tungsten τ_p=$\langle N_W \rangle / \langle \Phi_W \rangle$ was calculated from the average number of tungsten ions in the confined plasma $\langle N_W \rangle$ and the neutral production rate at the limiters $\langle \Phi_W \rangle$. A regression of τ_p on f_{ELM}, the spatially and temporally averaged parallel loss time from SOL to divertor $\langle\langle \tau_{SOL\to div} \rangle\rangle$ and D_{SOL} describes all values within a factor of 2 as is shown in Fig.5. It yields τ_p=1.4$\times$10^{-2} s $f_{ELM}^{-1.1} \langle\langle \tau_{SOL\to div} \rangle\rangle^{1.1} D_{SOL}^{0.1}$ for $[f_{ELM}]$=s^{-1}, $[\langle\langle \tau_{SOL\to div} \rangle\rangle]$=s and $[D_{SOL}]$=m^{2}s^{-1}. The dependence on D_{an}^{ETB} was negligible, since this parameter was only scanned in a range, where the neo-classical diffusion coefficient is dominant. Thus, τ_p increases almost linear with decreasing f_{ELM} and increasing $\langle\langle \tau_{SOL\to div} \rangle\rangle$, while the dependence on D_{SOL} is very weak. The effect of the SOL diffusion is twofold, driving a radial flux from the source location to the inside as well as to the outside. The weak dependence on D_{SOL} in this parameter range reflects the behaviour of the analyti-

cal solutions of the impurity transport equation [15,16], which can be calculated for the simple situation with temporally and spatially constant D_{SOL}, $\tau_{SOL\rightarrow div}$ and source rate. Thus, when knowing an experimental value for τ_p at a given ELM frequency, the most solid modeling output is the parallel loss time in the SOL provided that the radial transport during the ELM is well described. However, lower values of D_{SOL} produce more strongly peaked profiles near the source radius. The density profile near the source radius has a characteristic decay length $\lambda_{SOL,div}$=$\sqrt{D_{SOL}\tau_{SOL\rightarrow div}}$ and high impurity concentrations appear at the source location.
The model was applied to three H-mode discharges, with f_{ELM} =50, 100 and 200 Hz, where the erosion rates and the concentration inside the pedestal top are known. Due to the weak dependence of τ_p on D_{SOL}, the parallel losses were tuned to fit the measured concentrations of $c_{W,0.8}$ at r/a ≈0.8 for three values of D_{SOL}= 0.1, 0.32 and 1 m^2s^{-1} and fixed D_{an}^{ETB}=0.032 m^2s^{-1}. For the case with the lowest ELM frequency, the variation of the inter-ELM diffusion coefficient in the SOL has the strongest influence on the temporal average $\langle D_{SOL}\rangle$ during the ELM cycle. Here, the increase of D_{SOL} by a factor of 10 needs the largest change in $\langle\langle\tau_{SOL\rightarrow div}\rangle\rangle$ and can be compensated by a factor of 2 decrease of $\langle\langle\tau_{SOL\rightarrow div}\rangle\rangle$ to get the same particle confinement time (the W confinement would increase with increasing D_{SOL} at constant $\langle\langle\tau_{SOL\rightarrow div}\rangle\rangle$). The $\langle n_W\rangle$ profiles for the three D_{SOL} cases are shown in Fig.6 for #22901. The profile for D_{SOL} =0.1 m^2s^{-1}has a pronounced maximum around the source radius, and also for C and O very large concentrations around the source are found which might even lead to violations of the quasi-neutrality shortly after the ELM. Therefore, such low D_{SOL} values are less probable. Furthermore, measurements of the n_W decay lengths in the limiter shadow [17] of ≈ 5 mm also point in the direction of larger diffusion coefficients.

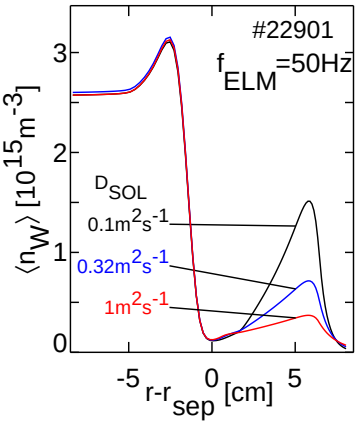

FIG. 6: Modeled radial profiles of $\langle n_W\rangle$ yielding the measured W concentration at $r/a = 0.8$ for the measured W influx for three different levels of the inter-ELM diffusion coefficient in the SOL.

Besides, the SOL transport issues, a strong effect of the ELM frequency on the average impurity gradient is found. For decreasing ELM frequency, the ratio $\langle n_{W,0.9}\rangle/\langle n_{W,sep}\rangle$ of the W density at $r/a = 0.9$ to the separatrix value increases somewhat stronger than linear, rising from 3.9 to 21. The suppression of the neo-classical W peaking due to ELMs depends on the strength and the duration of the increased diffusion in the model and details can only be tested by impurity density measurements around the ETB with good spatial and temporal resolution. Fast measurements of W concentrations around the ETB are very difficult and the method is still evolving [6]. In the present approach, all ELMs are identical in terms of transport coefficient increase. Each ELM reduces the tungsten content by $\Delta N_W/\langle N_W\rangle$=7-11%. This flushing of tungsten becomes strongest, when the density inside the pedestal top and in the SOL differs most. Finally, the prompt redeposition reduces the tungsten confinement by a factor of 2.5-3 for these discharges with B_T=-2.5 T.

5. Impurity transport in the ITER H-mode edge transport barrier

The focus in this section is on the perpendicular transport in the ETB and the consequences of a dominantly neo-classical impurity transport in the ETB between the ELMs. An attempt is made to calculate the average peaking of tungsten in the ETB of ITER plasmas for different ELM frequencies. It is an estimate for an ITER with tungsten PFCs in the main chamber, which might become relevant at a later stage of the ITER operation. The calculations are for the ITER-FEAT reference scenario for inductive operation. The pedestal top values, that fulfill the Q=10 requirement are $T_{e,ped}$=$T_{i,ped}$=4.8 keV, and $n_{e,ped}$=7.8×10^{19} m^{-3} [18]. Pedestal profiles were

added assuming a scaling of the pedestal width with R_{geo} [19].
Fig.7 shows the calculated neo-classical transport coefficients between ELMs and the assumed anomalous profiles of the diffusion coefficient D and of the drift parameter v/D. Additional impurities which contribute to the collisional transport of tungsten are helium with a concentration of $c_{\mathrm{He},0.9}$=2%, oxygen with $c_{0,0.9}$=0.9%, and Ar with $c_{\mathrm{Ar},0.9}$=0.05%. The neo-classical diffusion coefficient D_{neo} in the ETB is shown for each impurity. The values of D_{neo} are in the range 0.01-0.03 $\mathrm{m^2 s^{-1}}$and thus more than an order of magnitude below the typical values in ASDEX Upgrade. In order to have a dominant neo-classical impurity transport in the ETB the turbulent diffusion coefficient is reduced from 1 $\mathrm{m^2 s^{-1}}$at the pedestal top to an order of magnitude smaller values than D_{neo}, i.e. 1×10^{-3} $\mathrm{m^2 s^{-1}}$in the ETB, and increased again to 0.5 $\mathrm{m^2 s^{-1}}$in the SOL in order to avoid very small characteristic length scales in the divertor SOL. The ELM is again induced by the same recipe as before (upper black curve), a sudden switch on of a large diffusion coefficient decaying linearly within 1 ms.

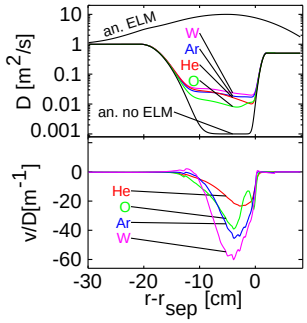

FIG. 7: Profiles of impurity diffusion coefficients and drift parameters for the modeling of edge transport in ITER-FEAT

The maximum permissible ELM energy loss in ITER is about ΔW_{ELM}=1 MJ. A rough estimate of the ELM frequency can be gained from the assumption that 1/3 of the power transported across the separatrix P_{sep} is exhausted within ELMs [20]. Using P_{heat}=120 MW and $P_{rad,core}$=0.25P_{heat} gives P_{sep}=90 MW and f_{ELM}=30 Hz. A scan of the ELM frequency was performed using f_{ELM}=33 Hz as the highest value and going down to f_{ELM}=5 Hz. For the case with highest ELM frequency, the influxes of oxygen and argon were set to have concentrations $c_{0,0.9}$=0.9% and $c_{\mathrm{Ar},0.9}$=0.05%. For Helium we considered the source due to fusion in the confined plasma, 100% recycling at the limiters and divertor recycling, which was calculated with a simple divertor chamber model which describes the pumping and recycling with decay times [21]. The parameters of the decay times were set to get a global confinement time of He τ^*_{He}=$\langle N_{He}\rangle/\Phi_{\mathrm{He},fus}$ of about 5 times the energy confinement time τ_E. For the other ELM frequencies the O and Ar influxes and the recycling model for He was left unchanged. Fig. 8 shows the modeled $\langle n_W\rangle$ profiles at the edge for the different ELM frequencies. All profiles are normalised to the same tungsten source rate. The absolute W densities can not be predicted and we just concentrate on the peaking within the separatrix. The peaking is very low at the higher frequencies and only changes remarkably when decreasing f_{ELM} to 10 Hz. At f_{ELM}=10 Hz the tungsten peaking across the pedestal is $\langle n_{W,0.9}\rangle/\langle n_{W,sep}\rangle$ ≈6 and at f_{ELM}=5 Hz the peaking factor is about 14. These values are in the range of peaking factors calculated for the ASDEX Upgrade ETB at about 20 times higher ELM frequencies. For argon and oxygen, the peaking is even weaker. Thus, the neo-classical impurity peaking in the ETB seems to be of much lower importance in ITER due to the low neo-classical transport coefficients leading to equilibration times much longer than the ELM repetition time, where it is assumed that the ELMs in ITER are effectively weakening the impurity gradient in the ETB.

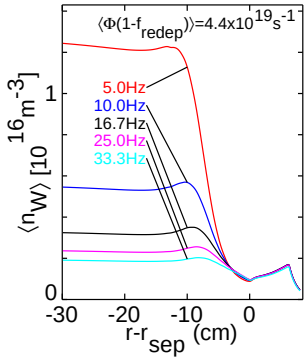

FIG. 8: W profiles in the ITER edge averaged over one ELM cycle. The profiles are for different ELM frequencies and are normalised to a prescribed effective source rate $\langle\Phi(1-f_{redep})\rangle$.

6. Conclusions

Fast measurements of the total erosion rates at the plasma facing components in ASDEX Upgrade have shown that at the outboard limiters (70±10)% of the erosion is due to ELMs, while at the inboard heat shield the contribution is lower at a level of (40±10)%. The ELM contribution does not depend on the energy loss during an ELM, i.e. less frequent larger ELMs cause the same contribution as more frequent smaller ELMs. The ratio of outboard to inboard erosion rates decreases, when the plasma is shifted to the inboard, however, the balance is different during an ELM and between ELMs with a stronger outboard contribution during an ELM.

For tungsten, the transport in the ETB is dominated by the effect of Coulomb collisions, since it has an even higher collisional diffusion coefficient than the light elements, for which the agreement with purely collisional transport could be deduced from direct measurements. The collisional transport produces a strong inward pinch and a respective peaking of tungsten which is relaxed during an ELM. When modeling the edge transport in ASDEX Upgrade with a 1D radial transport code, that treats the parallel losses in the SOL with volume loss rates, the impurity confinement time shows a strong reduction with increasing ELM frequency as experimentally observed. However, there is an equally strong dependence on the characteristic parallel loss time in the SOL, which is at present not well known and requires further measurements to restrict this parameter in the model. The dependence on the diffusion coefficient in the SOL is very weak and can hardly be determined from measured confinement times.

In the ETB of ITER, the collisional impurity diffusion coefficient is about a factor of 20 smaller than in ASDEX Upgrade. Thus the time to build up a strong edge gradient is substantially longer, however, the ELM frequency has to be kept high (around 20-30 Hz) in order to achieve small ELMs. Thus, the average edge peaking will be quite small, provided that the ELMs do not lead to a much smaller increase of the effective diffusion coefficient than used in the model.

References

[1] PÜTTERICH, T. et al., to appear in J. Nucl. Mater. (2010).
[2] PÜTTERICH, T. et al., Nuclear Fusion **50** (2010) 025012 (9pp).
[3] DUX, R. et al., in Proc. 20th IAEA FEC , Vilamoura, IAEA–CN–116, EX/P6–14, 2005.
[4] DUX, R. et al., Journal of Nuclear Materials **390-391** (2009) 858.
[5] PÜTTERICH, T. et al., Plasma Physics and Controlled Fusion **50** (2008) 085016.
[6] JANZER, M. A. et al., in Proc. 37th EUR Conf., Dublin, 34E(EPS), P–1.1046, 2010.
[7] PÜTTERICH, T. et al., in Proc. 36th EUR Conf., Sofia, 33E(EPS), P–1.158, 2009.
[8] DUX, R. et al., submitted to Nucl. Fus. (2010).
[9] DUX, R. et al., Journal of Nuclear Materials **363-365** (2007) 112.
[10] DUX, R., Rep. IPP 10/30, MPI für Plasmaphysik, Garching, 2006.
[11] EMMERT, G. A. et al., Phys. Fluids **23** (1980) 803.
[12] ECKSTEIN, W. et al., Rep. IPP 9/82, MPI für Plasmaphysik, Garching, 1993.
[13] THOMPSON, M. W., Phil. Mag. **18** (1968) 377.
[14] DUX, R. et al., in Proc. 36th EUR Conf., Sofia, 33E(EPS), O–5.056, 2009.
[15] POST, D. E. et al., in *Physics of Plasma-Wall Interactions in Controlled Fusion Devices*, ed. by BEHRISCH, R. et al., 627–692, 1986.
[16] DUX, R., Rep. IPP 10/27, MPI für Plasmaphysik, Garching, 2004.
[17] SCHUSTEREDER, W. et al., Journal of Nuclear Materials **363-365** (2007) 242.
[18] PEREVERZEV, G. N. et al., Nuclear Fusion **45** (2005) 221.
[19] KALLENBACH, A. et al., Journal of Nuclear Materials **337-339** (2005) 381.
[20] EICH, T. et al., Plasma Physics and Controlled Fusion **49** (2007) 573.
[21] KALLENBACH, A. et al., Nuclear Fusion **35** (1995) 1231.